Upscaling of U(VI) Desorption and Transport from Decimeter-Scale Heterogeneity to Plume-Scale Modeling

Final Report for Project

Award No. DE-SC0003681

Prepared by Gary P. Curtis, US Geological Survey, Menlo Park CA

With contributions from

Matthias Kohler, Ramakrishnan Kannappan, Martin Briggs and Fred Day-Lewis.

1: Introduction

Scientifically defensible predictions of field scale U(VI) transport in groundwater requires an understanding of key processes at multiple scales. These scales range from smaller than the sediment grain scale (less than 10 μm) to as large as the field scale which can extend over several kilometers. The key processes that need to be considered include both geochemical reactions in solution and at sediment surfaces as well as physical transport processes including advection, dispersion, and pore-scale diffusion. The research summarized in this report includes both experimental and modeling results in batch, column and tracer tests.

1.1 Objectives

The objectives of this research were to: (1) quantify the rates of U(VI) desorption from sediments acquired from a uranium contaminated aquifer in batch experiments;(2) quantify rates of U(VI) desorption in column experiments with variable chemical conditions, and(3) quantify nonreactive tracer and U(VI) transport in field tests.

1.2 The Naturita UMTRA Site

The field site is located at a former uranium mill, 3 km northwest of the town of Naturita, CO along the San Miguel River (Curtis et al., 2006). The former mill at Naturita processed uranium and vanadium at the site from 1939 until 1958. During 1977-79, mine tailings were removed from the site, and during 1996-98 contaminated vadose zone soils were excavated and transported offsite. Contaminated groundwater at the Naturita site occurs in thin alluvial deposits of the San Miguel River floodplain. Minerals in the aquifer consist primarily of quartz with smaller amounts of detrital feldspars, carbonates, magnetite, and fine clay-size materials (Davis et al., 2004b). Elevated concentrations of U(VI) and alkalinity are consistently observed below and downgradient of the former location of the U mill tailings. In September 1999, the average U(VI) concentration in the wells upgradient of the former facilities was 0.02 μM) which is below the USEPA drinking water standard of 0.13μM(USEPA, 2012). Impacted groundwater had U(VI concentrations between 2 and 6 μM. Alkalinity had a similar spatial pattern as U(VI), with a smaller range in concentration. The pH values ranged from 6.5 to 7.5, with an average pH of 7.1 (Curtis et al., 2006). The aquifer is generally suboxic, but not at equilibrium with respect to redox conditions (Davis et al., 2006). As

described below, the groundwater at the Naturita site also contained approximately 1 to 10 μM of ferrous iron (Fe(II)). The distribution of clay, silt, sand, pebbles, and cobbles within the aquifer is known to be very heterogeneous from tracer tests conducted in the aquifer (Curtis and Davis, 2006).

2. BACKGROUND

2.1 Site Description.

The groundwater at the Naturita site had a pH of 7.1, and alkalinity of 8meq/L (milli-equivalents per liter) and was in equilibrium with calcite. The water is near equilibrium with respect to calcite and the dissolved ferrous iron (Fe(II)) had an average concentration of 0.6 μM. Solutes in the aquifer migrate primarily parallel to the river from south to north because low permeability formations along the western boundary of the aquifer restrict groundwater flow.

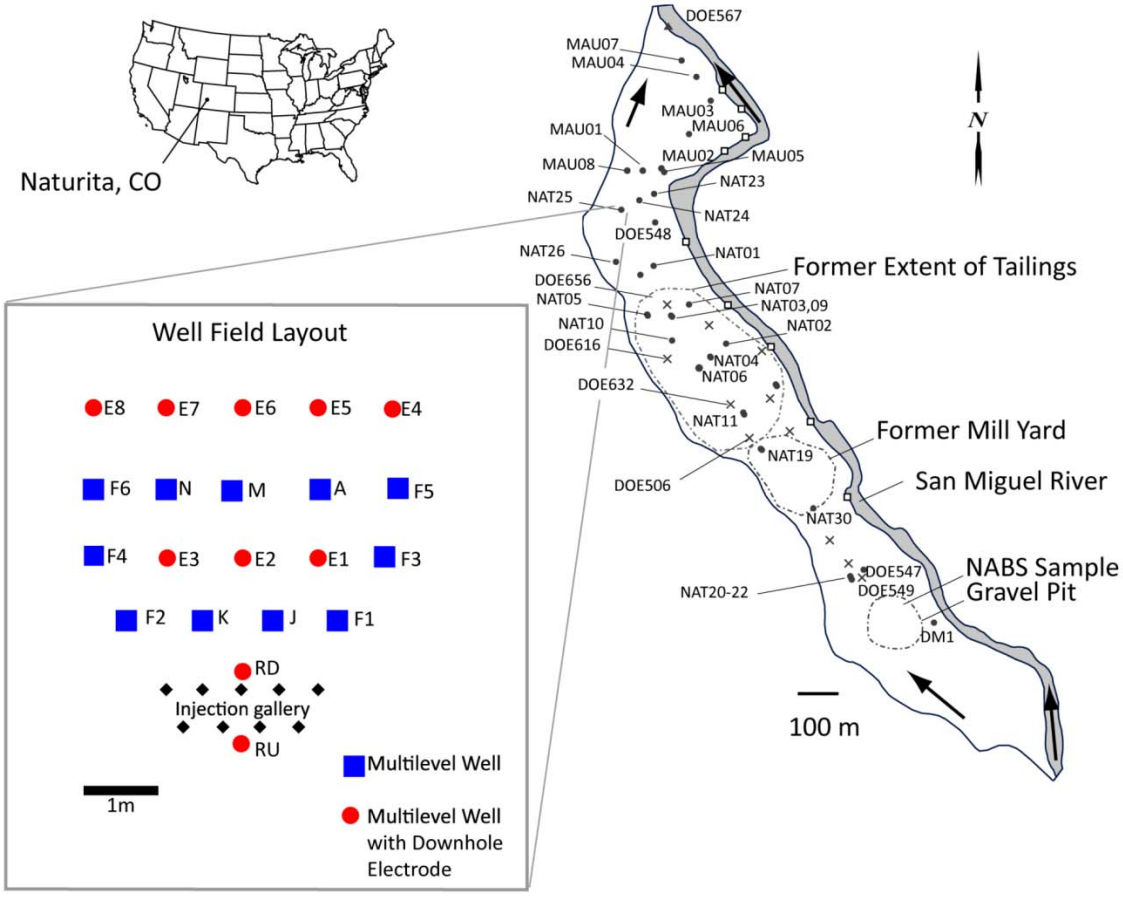

Figure 1. Locality map of the Naturita UMTRA site near Naturita CO. Flow is from bottom to top. Sediments used in the laboratory experiments were collected ~25m downgradient of the tracer test site.

2.2 Sediment Acquisition and Processing for Experiments

Sediment used in the laboratory experiments was collected from below the water table approximately 80 m down gradient of maximum U(VI) concentrations observed in the. The excavation site was approximately 25 m downgradient of the tracer test site described below. The groundwater at the excavation site had a dissolved uranium concentration of approximately 4 μM U(VI), a pH of 7.1 and alkalinity of approximately 9 meq/L. The sediments were excavated with a backhoe, homogenized and air dried in the field and shipped to the laboratory. The sediments were sieved into three fractions (<2mm, 0.25-2mm, and <0.25mmfor use in laboratory experiments.

2.1 Modeling Approach

The approach taken in this work was to conduct experiments at multiple scales and use batch experiments and reactive transport modeling to synthesize the results into a consistent framework across spatial scales ranging from 10^{-2} to 10^{3} m. Experiments were conducted in the laboratory using air dried sediments at the batch(<0.001m), column (0.1m) intermediate scale laboratory scale (~2.4m) and in tracer tests (~5m) conducted in the field. The results from these experiments are described below.

Reactive transport simulations were performed with the flow simulator MODFLOW-2005 (Harbaugh, 2005) and the reactive transport simulator PHT3D. PHT3D links the mass transport simulator MT3DMS with the aqueous geochemical reaction model PHREEQC by sequential operator splitting (Prommer, Barry, and Zheng 2003). Modifications were made to the PHREEQC input through the use of mixing factors to create a model with multiple immobile zones and a lognormal distribution of mass transfer rates (Greskowiak et al. 2010). The lognormal distribution was defined by the average mass transfer rate (μ) and the standard deviation of the distribution (σ). The basic equations describing the model are shown below:

$$\theta_m \frac{\partial C_m}{\partial t} + \sum_{j=1}^{N} \left(\theta_{im,j} \frac{\partial C_{im,j}}{\partial t} + \rho_b \frac{\partial S_{im,j}}{\partial t} \right) = \theta_m D \frac{\partial^2 C_m}{\partial x^2} - \theta_m v \frac{\partial C_m}{\partial x} \quad (1)$$

$$\theta_{im,j} \frac{\partial C_{im,j}}{\partial t} + \rho_b \frac{\partial S_{im,j}}{\partial t} = \alpha_j \theta_{im,j} (C_m - C_{im,j}) \quad (2)$$

$$cdf(\alpha, \mu, \sigma) = \frac{1}{2} + \frac{1}{2} erf \left[\frac{\ln(\alpha) - \mu}{\sigma \sqrt{2}} \right] \quad (3)$$

In equation 1 C_m is mobile aqueous concentration, θ_m is mobile porosity, $C_{im,j}$ is immobile aqueous concentration in immobile zone j, $\theta_{im,j}$ is immobile porosity for immobile zone j, $S_{im,j}$ is adsorbed concentration in immobile zone j, ρ_b is bulk density, D is hydrodynamic dispersion coefficient and v is mean velocity. Equation 2 is the mass balance equation for the j'th immobile zone where α_j is the first order mass transfer coefficient for the j'th immobile zone. Equation 3 indicates that the α values are drawn from the lognormal distribution with mean μ and variance σ. The multirate mass

transfer model described in equations 1 through 3 has been implemented in the reactive transport code PHT3D and was used in this study.

3. RESULTS

3.1 Batch Experiments and Modeling

A surface complexation model was developed from batch U(VI) desorption data from sediments collected at the Naturita UMTRA site. This approach was complicated by slow changes in alkalinity and pH that are likely caused by oxidation of sediment-associated Fe(II) present at 2μmol/g. In order to describe quantitatively the rate of U(VI) desorption, reactions responsible for changes in alkalinity and pH values observed during experiments needed to be taken into account. A conceptual model incorporating oxidation of Fe(II) to Fe(III) upon exposure of the aquifer sediments to atmospheric oxygen during drying accounted for the observed changes in alkalinity and pH values. The oxidized iron both precipitated to form iron-oxyhydroxide and produced protons according to the reaction.

$$Fe^{2+} + 2.5H_2O + 0.25O_2 = Fe(OH)_3 + 2H^+ \qquad 4$$

$$2CaCO_3 + 2H^+ \rightarrow 2Ca^{2+} + 2HCO_3^- \qquad 5$$

which yields the overall reaction

$$Fe^{+2} + 2.5H_2O + 0.25O_2 + 2CaCO_3 -> Fe(OH)_{3(S)} + 2Ca^{+2} + 2HCO_3^- \qquad 6$$

This overall reaction increases the alkalinity of the artificial groundwater and some of the HCO_3^- produced in equation 6 dissociates to produce H^+ and CO_3^{-2} which lowers the pH. This reaction model accounted for the increase in pH and the decrease in alkalinity observed in all of laboratory experiments conducted in this study.

Batch experiments were conducted in the laboratory to evaluate the equilibrium distribution of uranium between the solid and aqueous phases for each of the three size fractions (<0.25mm, 0.25-200mm and <200mm). These continually mixed experiments were conducted over long periods of time (~ 60-90 days) to improve the likelihood that equilibrium was approached by the end of the experiment. In addition, a wide range of solid to liquid ratios were used to better account for U(VI) sorption over a range of sorption site and aqueous concentrations. Alternative adsorption reactions listed in Table 1 were also considered in developing equilibrium batch adsorption the model.

Figure 2 illustrates the temporal evolution of the geochemical conditions observed in batch experiments for a less than 2 mm grain size sample that was contacted with artificial groundwater for a period of 2600 hours. The results show that the concentrations of all of the analytes including the major ions pH alkalinity and uranium concentrations initially changed rapidly and then subsequently changed slowly over time. The initial rapid changes in concentration wereattributed to dissolution of salts that precipitated when the sediments were dried in the field. With increasing

time the rate of change of all solutes slowed with time and often resulted in difficultly in assessing where equilibrium could be assumed. One approach to estimating the equilibrium constants would be to assume that the last concentrations measured in the batch reactors represented equilibrium and that all other measurements represented kinetic departure from equilibrium. In this work we assumed that the kinetic release of uranium could be controlled by the evolution of the major ion chemistry, particularly the calcium and alkalinity values, that was observed in all of the batch experiments. This alternative approach of calculating the ion activity product for the uranium adsorption reactions circumvents the interferences introduced by slow changes in the inorganic geochemistry and maximizes the use of the data for the purpose of estimating equilibrium constants.

Eleven alternative surface complexation reactions were tested to determine which reaction stoichiometry best described adsorption of uranium by different sediment size fractions. The ion activity products of the adsorption reactions were calculated from the observed aqueous composition and the calculated concentrations in the surface complexes. The changes in the ion activity products of the adsorption were used to evaluate the approach to equilibrium for each postulated adsorption reaction. Speciation calculations were performed with PHREEQC using the NEA database (Guillaumont et al,2003). These eleven alternative adsorption reactions considered are listed in Table 1. Diffusive mass-transfer could have accounted for increases in dissolved U(VI) after during the first ~100 hours of the experiment but further increases could be controlled by the decrease in pH and increase in alkalinity.

Table 1. Adsorption reactions tests for the kinetic approach to equilibrium

Model	Reactants		Products
A1	$>T(OH)_2 + UO_2^{+2}$	=	$>TO_2H_2UO_2^{+2}$
A2	$>T(OH)_2 + UO_2^{+2}$	=	$>TO_2HUO_2^{+} + H^{+}$
A3	$>T(OH)_2 + UO_2^{+2}$	=	$>TO_2UO_2 + 2H^{+}$
A4	$>T(OH)_2 + UO_2^{+2} + H_2CO_3$	=	$>T(OH)_2UO_2HCO_3^{+}$
A5	$>T(OH)_2 + UO_2^{+2} + H_2CO_3$	=	$>T(OH)_2UO_2CO_3$
A6	$>T(OH)_2 + UO_2^{+2} + H_2CO_3$	=	$>TO_2HUO_2CO_3^{-} + H^{+}$
A7	$>T(OH)_2 + UO_2^{+2} + H_2CO_3$	=	$>TO_2UO_2CO_3^{-2} + 2H^{+}$
A8	$>T(OH)_2 + UO_2^{+2} + 2H_2CO_3$	=	$>TO_2H_3UO_2(CO_3)_2$
A9	$>T(OH)_2 + UO_2^{+2} + 2\ H_2CO_3$	=	$>T(OH)_2UO_2(CO_3)_2^{-2}$
A10	$>T(OH)_2 + UO_2^{+2} + 2\ H_2CO_3$	=	$>TO2HUO_2(CO_3)_2^{-3} + H^{+}$
A11	$>T(OH)_2 + UO_2^{+2} + 2\ H_2CO_3$	=	$>TO2UO_2(CO_3)_2^{-4} + 2H^{+}$

The transient concentrations observed in batch desorption experiments are illustrated in Figure 2. For each of the selected solutes concentrations change rapidly during the first 600 hours followed by slower rates of change for uranium alkalinity and calcium whereas pH is nearly stable during this period. The slow changes in concentration suggest that equilibrium was not attained even during the first 2600 hours the experiment. However the observed changes in the concentration of major species does not necessarily demonstrate uranium desorption disequilibrium. The processes controlling major ions may be very different from those processes affecting uranium desorption. A

more robust approach to evaluate disequilibrium is to calculate the ion activity product for alternative adsorption reactions. Results of this calculation are shown in Figure 3 which shows the ratio of the ion activity product at any time to the value observed at the end of the experiment. Calculation shows significant scatter in the calculated ion activity products during the first 400 hours which could result from slow rehydration of the sediments, slow dissolution reactions or mass transfer limitations. However, during the last three sampling periods between 666 hours in 2600 hours the ion activity product ratio is essentially constant even though the concentrations vary as shown in Figure 2. This constant ratio is therefore good evidence that equilibrium is achieved after 666 hours even though individual solute concentrations were still changing. These latter observations were used develop surface complexation models for uranium adsorption by the sediments. Development of these models used additional data at smaller solid to liquid ratios (not shown).

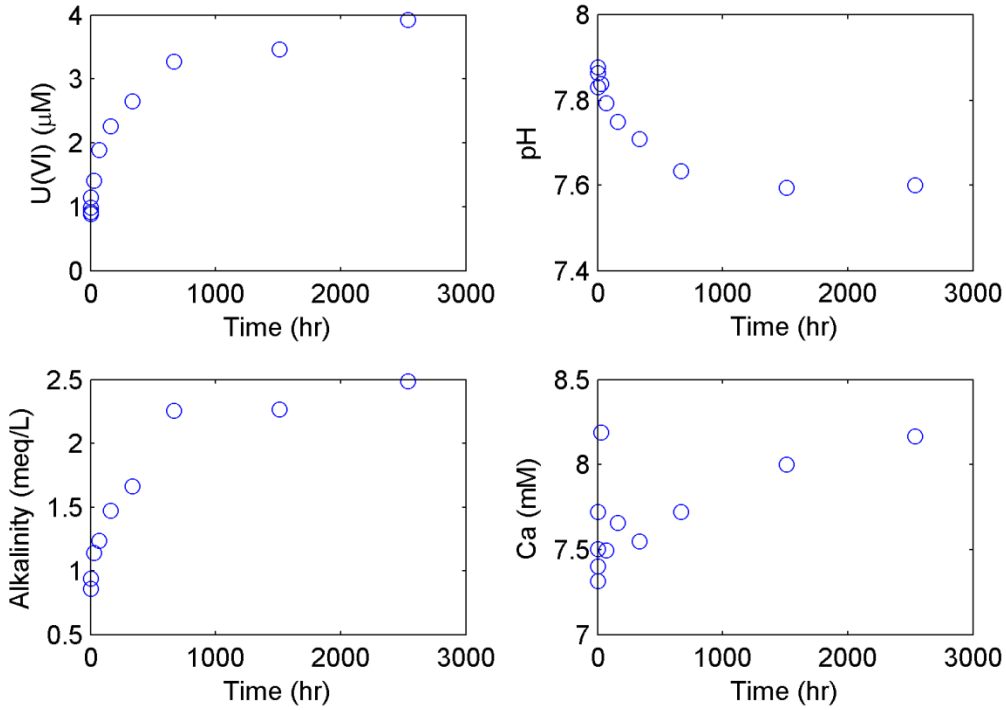

Figure 2. Concentrations of uranium pH alkalinity and calcium versus time observed in the batch experiments containing 1000 g/L of the <2mm Naturita sediments.

The transient concentrations observed in batch desorption experiments are illustrated in Figure 2. For each of the selected solutes concentrations change rapidly during the first 600 hours followed by slower rates of change for uranium alkalinity and calcium whereas pH is nearly stable during this period. The slow changes in concentration suggest that equilibrium was not attained even during the first 2600 hours the experiment. However the observed changes in the concentration of major species does not necessarily demonstrate uranium desorption disequilibrium. The processes

controlling major ions may be very different from those processes affecting uranium desorption. A more robust approach to evaluate disequilibrium is to calculate the ion activity product for alternative adsorption reactions. Results of this calculation are shown in Figure 3 which shows the ratio of the ion activity product at any time to the value observed at the end of the experiment. Calculation shows significant scatter in the calculated ion activity products during the first 400 hours which could result from slow rehydration of the sediments, slow dissolution reactions or mass transfer limitations. However, during the last three sampling periods between 666 hours in 2600 hours the ion activity product ratio is essentially constant even though the concentrations vary as shown in Figure 2. This constant ratio is therefore good evidence that equilibrium is achieved after 666 hours even though individual solute concentrations were still changing. These latter observations were used develop surface complexation models for uranium adsorption by the sediments. Development of these models used additional data at smaller solid to liquid ratios (not shown).

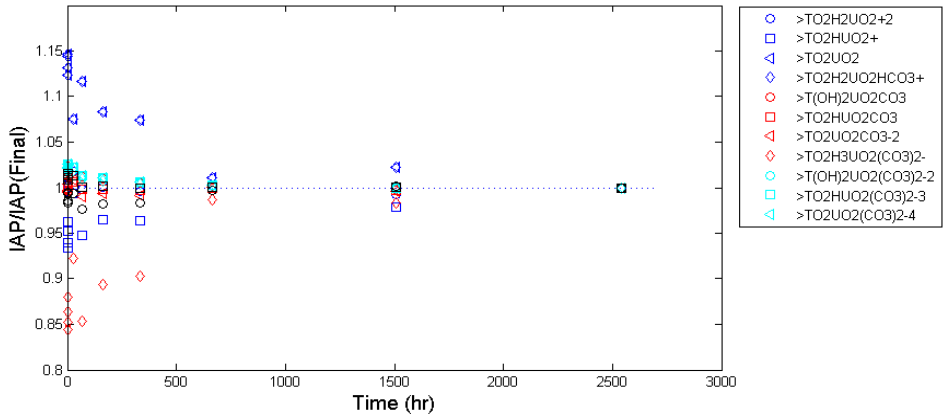

Figure 3. Calculated ion activity product ratios for alternative surface complexation reactions calculated for 1000g/L suspensions of the <2mm sample in artificial groundwater and in equilibrium with 0.2 atm CO_2.

Six alternative surface complexation models were calibrated to the batch desorption data. These alternative models tested various reaction stoichiometries for each size fraction as shown in Table 2. Two one-site/one-reaction models (Models 1 and 2) were calibrated to data for all three experimental conditions and the results are listed in Table 2. For both Models 1 and 2 the calibrated logK results are fairly consistent (within ~0.4 log units) for the three size fractions. For both models, however, the largest LogK value was estimated for the <2mm composite size fraction. Generally, the logK value for the composite sample would be expected to be bounded by or equal to the average of the logK values for the two size fractions. However the detailed assessment of the differences among the logK values needs to account for uncertainty bounds of the estimated logK values which was not considered in this study.

Table 2. Alternative surface complexation models calibrated to uranium desorbed in artificial groundwater

Model	Reaction	Size Fraction					
		< 0.25 mm		0.25 <2mm		<2mm	
	One site/one reaction models	Log K	fit[a]	Log K	fit	Log K	fit
1	$TOH + UO_2^{+2} = TOUO_2^{+} + H^{+}$	3.25	1.18	3.48	2.38	3.67	0.59
2	$TOH + UO_2^{+2} + H_2CO_3 = TOUO_2CO_3^{-} + 3H+$	-7.84	1.19	-7.68	4.62	-7.53	1.95
	One site/two reaction models						
3	$TOH + UO_2^{+2} = TOUO_2^{+} + H^{+}$	3.06			NI[b]	3.55	
	$TOH + UO_2^{+2} + 2H_2CO_3 = TOHUO_2(CO_3)_2^{-2} + 3H^{+}$	-12.0	0.51			-11.9	0.41
4	$TOH + UO_2^{+2} + H_2CO_3 = TOHUO_2CO_3^{-} + 2H^{+}$	-1.17			NI		NI
	$TOH + UO_2^{+2} + H_2CO_3 = TOUO_2CO_3^{-} + 3H^{+}$	-7.95	0.55				
5	$TOH + UO_2^{+2} + H_2CO_3 = TOHUO_2CO_3^{-} + 2H^{+}$		NI		NI	3.55	
	$TOH + UO_2^{+2} + H_2CO_3 = TOUO_2CO_3^{-} + 3H^{+}$					-11.8	0.48
	Two Sites/One Reaction						
6	$TOH + UO_2^{+2} = TOUO_2^{+} + H^{+}$		NI		NI	7.50	
	$XOH + UO_2^{+2} = XOUO_2^{+} + H^{+}$					3.35	0.30

a.) Fit is the sum of weighted squared residuals normalized by the number of degrees of freedom as calculated by FITEQL.

b.) NI – No improvement relative to the one site/one reaction model for this reaction

3.2 Column Experiments and Modeling

Four column experiments were conducted to quantify uranium desorption rates under well-controlled flow conditions. The columns varied from 6 to 10 cm in length and were packed with either the less than 2 mm composite sediment, the less than 0.25 millimeter sediment, or the 0.25 – 2mm size fraction. Artificial groundwaters were designed to mimic the field site which contains calcite but also allowing for varying partial pressures of carbon dioxide and therefore pH. The characteristics of the columns used in this study are summarized in Table 3 and the detailed composition of the groundwater is listed in Table 4.

Table 3. Conditions for column experiments

Experiment	Size Fraction	Mass [g]	Packed bed length [mm]	Porosity n [%]	Artificial Groundwater (see Table 2)	Headspace CO_2
COL30	< 2mm	39.2	64.7±0.3	39.39	AGW-25	$3.73 \cdot 10^{-4}$
COL31	< 2mm	40.4	64.5±0.5	36.84	AGW-25-2	2.0^{-2}
COL32	250µm – 2mm	65.3	102.8±0.3	36.48	AGW-25 AGW-25-2	$3.73 \cdot 10^{-4}$ & $2.\ 10^{-2}$
COL33	<250µm	39.5	64.5±0.5	38.69	AGW-25-2-Si AGW-25-Si	$3.73 \cdot 10^{4}$ & $2.\ 10^{-2}$

Table 4. Compositions of the artificial groundwaters used in the column experiments

	Na^+	K^+	Mg^{2+}	Ca^{2+}	ClO_4^-	SO_4^{-2}	CO_3^{-2}	$SiO_4H_2^{-2}$	pCO_2	pH
	[mM]	[mM]	[mM]	[mM]	[mM]	[mM]	[mM]	[mM]	[atm]	SU
AGW-25	24.3	0.25	2.67	5.73	16.5	12.1	0.610	0.0	$3.73 \cdot 10^{-4}$	7.91
AGW-25-Si	24.3	0.25	2.67	5.73	16.5	12.1	0.610	0.20	$3.73 \cdot 10^{-4}$	7.91
AGW-25-2	21.2	0.25	2.67	5.73	13.3	12.1	3.85	0.0	$2.00 \cdot 10^{-2}$	6.99
AGW-25-Si-2	21.2	0.25	2.67	5.73	13.3	12.1	3.85	0.20	$2.00 \cdot 10^{-2}$	6.99

Four column experiments were conducted to quantify uranium desorption rates under well-controlled flow conditions. The columns varied from 6 to 10 cm in length and were packed with either the less than 2 mm composite sediment, the less than 0.25 millimeter sediment, or the 0.25 – 2mm size fraction. Artificial groundwaters were designed to mimic the field site which contains calcite but also allow for varying partial pressures of carbon dioxide and therefore pH.

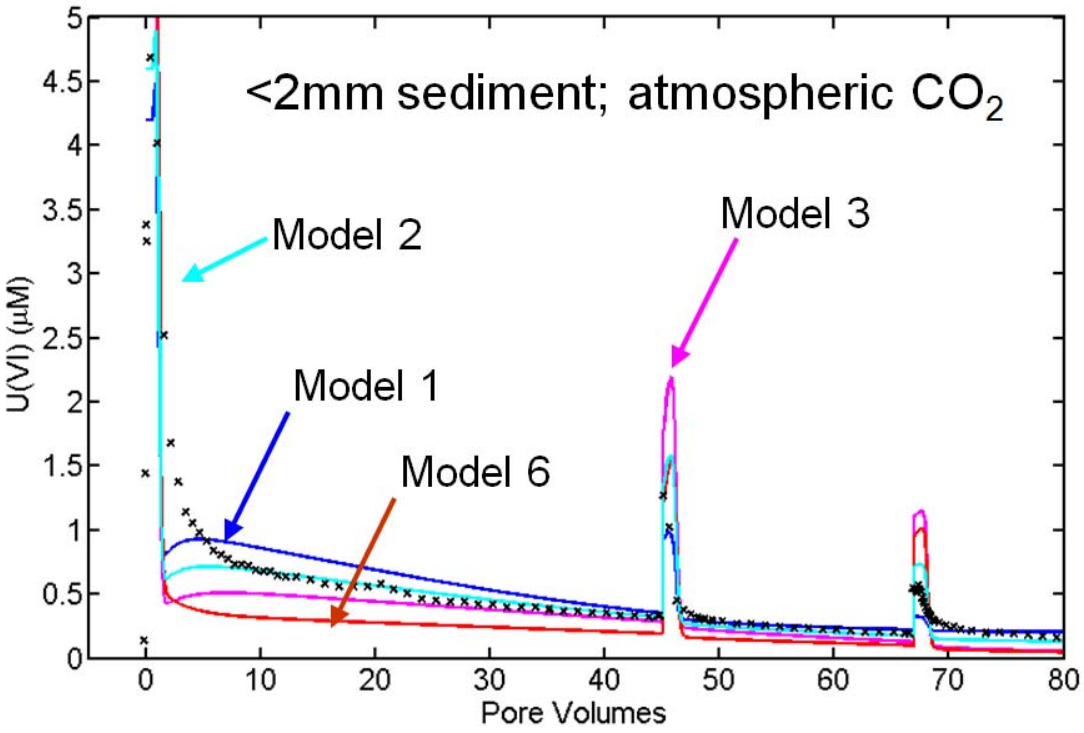

Figure 4. Comparison of observed data with reactive transport simulations experiment COL30 using the mobile-immobile zone mass transfer models listed in Table 1

An illustrative example comparing the experimental data with alternative model simulations is shown in Figure 4 for experiment COL30. The data show a rapid increase of the U(VI) concentration to 4.7µM in the first pore volume. This increase results from release of U(VI) from both evaporated groundwater and from sorption sites. The U(VI) concentration decreases to less than 1 µM in the first 4 pore volumes and continues to gradually decrease until 46 pore volumes. At that time, the flow was interrupted for 124 hours allowing additional time for desorption to occur in the column. Similarly, flow was interrupted for 290 hours after 68 pore volumes and again the U(VI) concentration increased. Finally, the concentration decreased when flow was resumed.

Reactive transport modeling was used to simulate the experimental results. These simulations considered four different surface complexation models listed in Table 2. Rate limited mass transfer was simulated using the multirate mass transfer model and the results shown in figure 4 for four different models generally reproduce the observed changes including the rapid increase in uranium concentration at time zero, the relatively rapid decrease in concentration when flow started in the column and the long tailing observed after the first few portable. The alternative models show slightly different behavior when considered at a detailed scale. For example Model 1 over predicts the U(VI) concentration for the first 46 pore volumes but then under predicts the U(VI)

concentration rebound observed at the stop flow events at 47 hours. Similarly, the concentration is overpredicted 48 and 68 pore volumes and under predicted during the stop flow event. In contrast, Model 3 under-predicts the U(VI) observations at early times but over predicts the U(VI) concentration during the stop flow events. This successful bracketing of the U(VI) desorption data is encouraging because it is becoming more commonly recognized that modeling complex reactive transport scenarios should embrace a multi-model approach.

3.3 Decimeter Experiments and Modeling

This work simulates uranium transport observed in tank experiments conducted at the Colorado School of Mines (Miller et al., 2013). Two uranium desorption experiments were conducted in tanks with sediments from the Naturita site. The sediments were sieved into size fractions and packed to create a known flow field. The first tank (Tank 1) used a homogeneous packing of <2 mm sieved fractions and the second tank (Tank 2) was packed with lenses of fine (<0.25 mm) and coarse (0.25 to 2 mm) materials to create low and high conductivity zones respectively as illustrated in Figure 5. The tanks were packed using air dried sediments collected from the Naturita site and were slowly resaturated from the bottom by introducing artificial groundwater into the tanks(Miller et al., 2013). This slow rehydration probably reduced the magnitude of the observed alkalinity disequilibrium described above for the batch and column experiments.

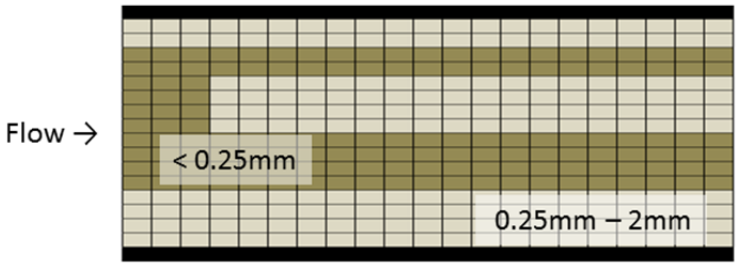

Figure 5. Packing geometry for the tank experiments conducted with Naturita sediments. The tank was 2.2m long and 0.6m high. Sample were collected from ports distributed along flowpath and from the composite tank effluent.

Flow through the tank was controlled by constant head boundary conditions. The artificial groundwater that used in the tank used a synthetic groundwater in equilibrium with atmospheric CO_2. The ionic composition of this water in the tank experiment closely matched the groundwater composition in the field to the extent possible. As described by Miller et al. (2013) the composition was varied slightly so that the tanks could be run under atmospheric partial pressures of CO_2 rather than the partial pressures observed in the field which are approximately 5% CO_2. Flow in the tank was interrupted several times to evaluate the concentration rebound resulting from rate-limited desorption of U(VI) from the sediments.

The multirate mass transfer model (Haggerty and Gorelick, 1995; Greskowiak et al., 2011) was used to simulate the reactive transport in the tank experiments as described above. In this approach, the mobile zone is assumed to exchange solutes with multiple immobile zone each having a unique

immobile porosity and mass transfer coefficient (eg Equations 1-3). In all of the simulations, the total immobile porosity was divided equally between the simulated immobile zones. The number of immobile zones was increased and the volume of each immobile zone was decreased until simulation results did not significantly change with additional immobile zones. Chemical equilibrium was assumed in each individual immobile zone and in the mobile zone but physical disequilibrium between the mobile and immobile zones was included. Sorption site concentration was determined from sediment surface area measured by BET and sorption site density of 2.3sites/nm^2. (Davis and Kent, 1990). Dispersivity values were set to one half of the grid spacing to minimize dispersive mixing in the simulations. The remaining parameters were determined by optimizing the model to specific sets of experimental data. PHT3D simulation results were processed in MATLAB to produce flow-weighted breakthrough curves from the concentrations in the last column of model cells.

Initially, the flow field for Tank 2 required additional estimated parameters because of the hydraulic conductivity heterogeneity. The zones of high and low conductivity were first grouped into six facies with varying bulk properties including porosity and packed density. Three high conductivity facies shared a hydraulic conductivity, mobile porosity, and μ value (equation 3) for the mass transfer rate distribution. The same was done for the three low conductivity facies. Initial simulations showed that it was not possible to match both total flow in the tank and the early arrival of tracer. The arrival time of the first experimental Br peak in the tank effluent was earlier than in the simulation using the known K, gradient and porosity. Even in the extreme case based on assuming that all the flow traveled through the high conductivity zone for reasonable porosity values the simulated Br arrived after first the observed Br peak arrived. To address this issue, the model was modified to include two short circuit zones at the top and bottom of the tank to allow for fast flow to bypass the emplaced high and low conductivity zones. Possible explanations for the existence of the short circuit flow path in the experimental setup include flow along the walls of the tank, uneven compaction during packing, and uneven settling when the tanks were initially flooded with artificial groundwater. An additional facies was added to the model to represent the short circuit zones. Although double peaks in the Br breakthrough are possible with certain sets of hydraulic and mass transfer parameters, the solution space of those parameters is very small and do not match the general shape of the breakthrough curve. The short circuit approach provided a simpler more plausible explanation that also reasonably fit the data.

Simulations of U(VI) transport in Tank 1 began by estimating overall hydraulic conductivity in the tank to establish a model flow field and as a model parameter. Since the flow rate was experimentally determined, the overall head for the tank was proportional to the overall hydraulic conductivity. The overall hydraulic conductivity for each tank was an estimated parameter (Tank 1) or a combination of estimated parameters (Tank 2). For Tank 1, the hydraulic conductivity, fraction of the pore space which was accessible to flow (mobile pore fraction) and the average of the mass transfer rate distribution were estimated by minimizing square of the residuals between the experimental and simulated breakthrough curve for Bromide (Br) tracer. The resulting fit produced good agreement for Ca and Mg concentrations in the effluent.

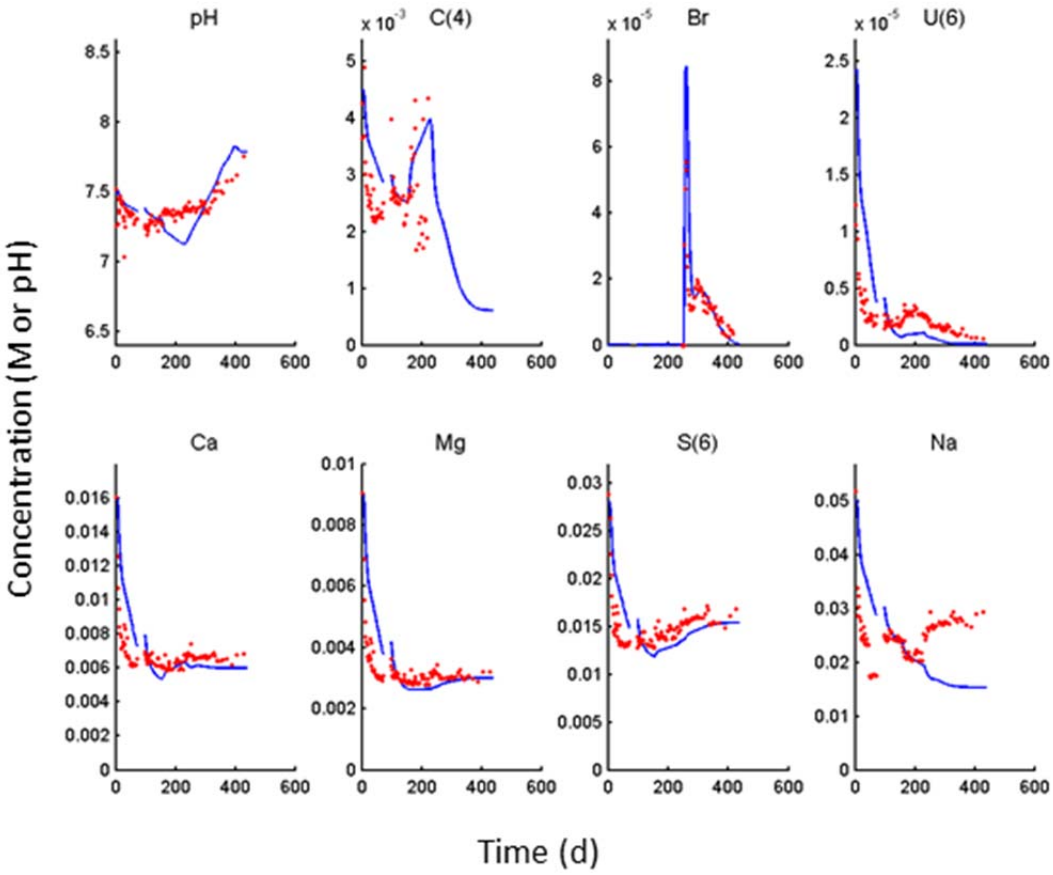

Figure 6. Calibration results for pH, Alkalinity (C(4)), Br tracer, U(VI) and major ions observed in Tank 2 effluent. Discontinuities in the simulations represent flow interruption events.

After the flow parameters were established for Tank 1, a significant difference between the observed and simulated alkalinity remained. The observed alkalinity was initially much higher than predicted. As described above, the additional alkalinity could be explained by the oxidation of Fe^{+2} and dissolution of calcite as described above. However, to simulate the transient increase in alkalinity, the ion exchange model was modified to include the exchange of $CaHCO_3^+$ rather than including Fe(II) oxidation. The iron oxidation would have occurred during the initial drying of the sediment and not during the transport experiment. This revised ion exchange was recalibrated to provide a reasonable match to the experimental data. Surface complexation constants for model 1 (Table 2) were increased by 0.32log units to fit to major ion concentrations observed in Tank 1.

The surface complexation model developed in Tank 1 was used in Tank 2 to predict U(IV) and major cation breakthrough curves as shown in Figure 6. This model gave good predictions for pH, uranium and major ions with the exception of Na at late times. However, attempts to predict breakthrough at the ports produced poor agreement (results not shown). This is likely because the actual small scale heterogeneity in the tank is more complex than was assumed in the model. Although samples were collected at ports throughout the tank, the data were somewhat sparse and

the size of the facies assumed for the model were too large to capture the complexity of the data from the ports. The facies would need to be broken into smaller facies and more parameters introduced to capture the granularity of the port data.

Although the model breakthrough curves at individual ports differed from the experimental data, certain phenomena were seen in both the model and experimental data. In the column experiments described above (section 3.2), stopped flow events produced distinct rebound peaks in the breakthrough consistent with a rate-limited in uranium desorption. However, the breakthrough curve for Tank 2 does not show significant rebound, but an examination of specific ports especially near the inlet of the tank shows rebound. Ports downgradient show progressively less rebound as shown in Figure 7. Near the outlet of the tank the rebound seen in the ports is minimal. Both the model and port data show this behavior.

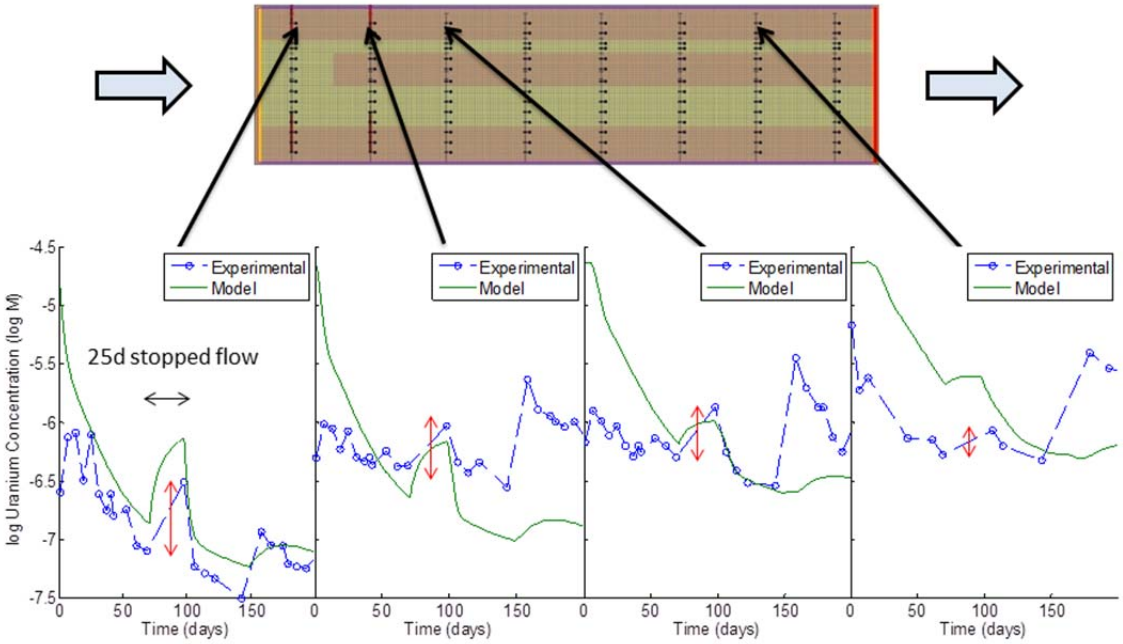

Figure 7. Observed and simulated concentration rebound during stop flow events at four locations along a flow path in tank 2.

An examination of the U(VI) concentration in different zones in the model explains this behavior. The concentration gradient is the driving force for diffusive mass transfer between mobile and immobile zones in the tank. This concentration gradient decreases from the inlet to the exit of the tank. At the front of the tank U(VI)-free water enters and leaches U(VI) from the contaminated sediment. As a result, U(VI) desorption occurs from the immobile to the mobile porosity near the inlet of the tank. As the water moves downgradient the mobile zone U(VI) concentration increases and therefore the driving force for mass transfer from the mobile and immobile zones decreases. The model shows that at the front of the tank the immobile zone U(VI) concentration is 50-70 times higher than the mobile zone aqueous concentration. At the end of the tank the mobile zone concentration is only 3-5 times greater than the corresponding immobile zone concentration. The model uses the difference in mobile and immobile zone concentration as the driving for mass

transfer between these two zones. The simulation results in Figure 8 show the U(VI) concentrations in the tank effluent are strongly controlled by mass transfer for all three mass transfer parameter values. As the mass transfer coefficient is increased, the simulated U(VI) concentration at the end of the tank increases because of the increasing mass transfer rates. Eventually the higher U(VI) concentration in the effluent would decrease the time to completely leach the U(VI) from the tank.

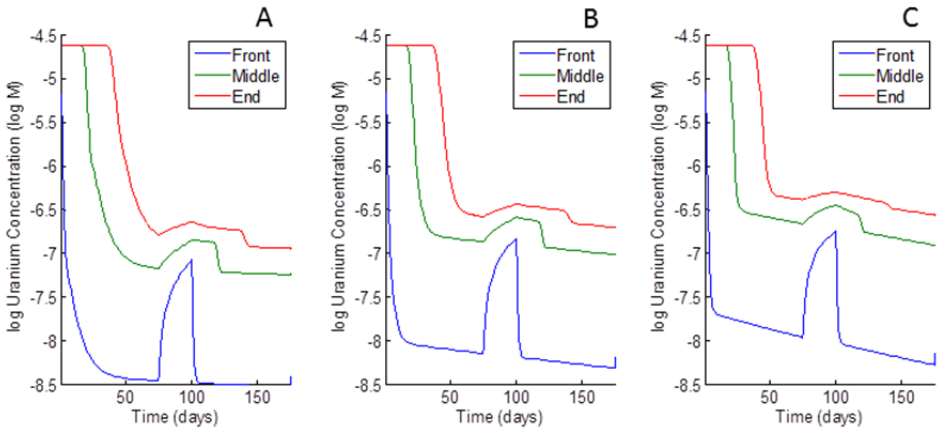

Figure 8. Simulated concentration rebound at three locations in the tank and for a mass transfer coefficients equal to 0.1, 1 and 10 for panels A-C respectively. The simple mobile-immobile zone was used for illustrative purpose.

3.4 Field Tracer Test Experiments

A field scale tracer test experiment was conducted by injecting high conductivity groundwater into the injection gallery (Figure 1). Specifically, NaCl was added to dechlorinated drinking water to increase the electrical conductivity from an initial value of 1780 µS/cm to 8400 µS/cm. The high conductivity water was injected for 15 days followed by fresh water with a conductivity equal to 365 µS/cm for 12 days. The tracer test was monitored by collecting traditional groundwater samples from the 21 multilevel monitoring wells shown in Figure 1. The electrical conductance of groundwater samples collected from each of the multilevel monitoring wells was measured in the field daily to obtain the fluid conductivity of each sample. Bulk conductivity in the aquifer was also measured using downhole electrodes as described in Briggs et al. (2014). This bulk conductivity measures conductivity associated with the groundwater, the aquifer sediments, and water in immobile zones (Figure 9B). By combining the fluid conductivity with the bulk conductivity it is possible to parameterize the common dual domain mass transfer model

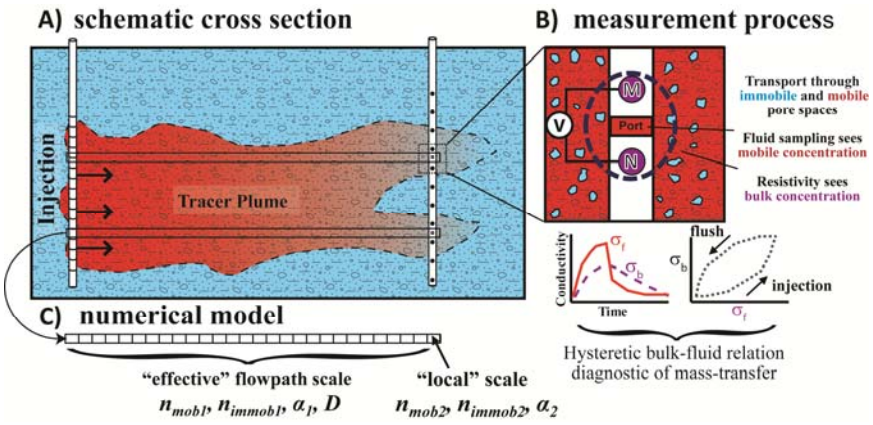

Figure 9 Schematic cross-section of (A) a generic field-scale tracer test (not to scale); (B) the local scale where co-located fluid (σ_f) and bulk (σ_b) conductivity measurements are performed (Briggs et al, 2013).

Measured values of the fluid and bulk conductivity were used to calibrate a mobile-immobile zone transport model. Figure 10 illustrates that this model matches both fluid and bulk conductivity and provides direct evidence for the presence of immobile zones at the local scale. Models were calibrated simultaneously to the fluid conductivity (σ_f, red) collected with a conductivity probe and bulk conductivity (σ_b , blue) collected by electrical resistivity profiles as shown in Figure 10. Hysteresis patterns, indicating mass transfer at the local scale, existed to varying degrees at the observation wells. All patterns were well simulated the mass transfer model (Briggs et al., 2014). This approach has allowed estimation of both flowpath and local scale mass transfer parameters in the subsurface for the first time.

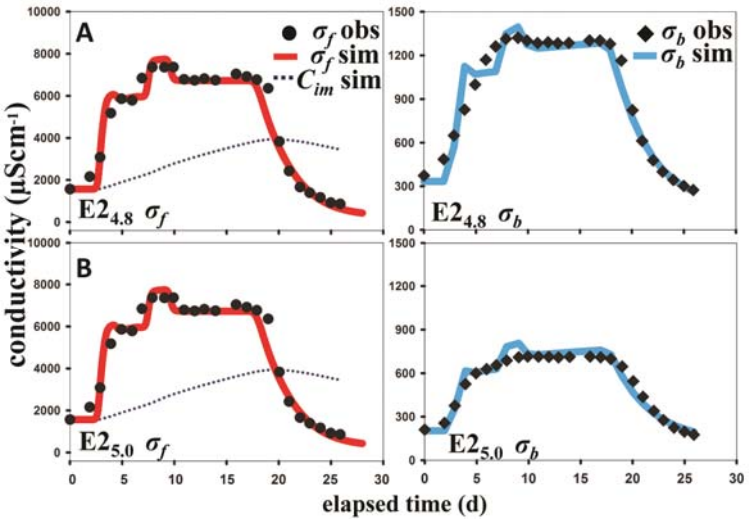

Figure 10. Observed and calibrated fluid and bulk electrical conductivities at well E2 at depths of 4.8 and 5.0 meters. The simulated concentration of solute in the immobile zone C_{im} is also show.

Application to Uranium Transport

This rich dataset is currently being used to estimate the spatial variability of the hydraulic conductivity at the tracer test site. This work is being performed by doctoral student under the supervision of Dr. Fred Day-Lewis (USGS; Storrs, CT). The hydraulic conductivity field estimated from the nonreactive tracer will be used to interpret the second tracer test which was a uranium desorption tracer test. This second test was conducted to evaluate rates of uranium desorption and was designed to reproduce the condition of the geophysical test to the maximum extent possible. Specifically, the same volume of water was injected at the same rate in the two tests. The uranium desorption tracer test did not use high concentrations of sodium chloride because of the likely interference with uranium reactions and groundwater. The injection for the uranium transport test used dechlorinated drinking water and the intent was to initiate uranium desorption. Approximately 1800 samples were collected during the 60 day field test. A representative subsample (~850) of these have been analyzed for U(VI), pH, akalinity, major ions and Cl^- as a tracer. Hydraulic conductivity field(s) are being estimated from the time-lapse geoelectrical data collected at wells E1-E8 and chloride data. These hydraulic conductivity fields will be coupled with reactions influencing U(VI) desorption using parameters determined from both the field observations and from laboratory experiments.

4. Products

Publications:

Fox, P. M., J. A.Davis, M. B.Hay, M. E.Conrad, K. M.Campbell, K. H.Williams, and P. E.Long (2012), Rate-limited U(VI) desorption during a small-scale tracer test in a heterogeneous uranium-contaminated aquifer, Water Resour. Res., 48, W05512, doi:10.1029/2011WR011472. *(Dr Hay was supported by this project when he contributed to this manuscript).*

Briggs, M. A., F. D. Day-Lewis, J. B. T. Ong, G. P. Curtis, and J. W. Lane (2013), Simultaneous estimation of local-scale and flow path-scale dual-domain mass transfer parameters using geoelectrical monitoring, Water Resour. Res., 49,5615–5630, doi:10.1002/wrcr.20397. *(Dr. F.D. Day-Lewis was a co-PI on this project).*

Briggs, M. A., F. D. Day-Lewis,J. B. Ong, J. W. Harvey, andJ. W. Lane (2014), Dual-domain mass-transfer parameters from electrical hysteresis: Theory and analytical approach applied to laboratory, synthetic streambed, and groundwater experiments, Water Resour. Res., 50, 8281–8299, doi:10.1002/2014WR015880. *(Dr. F.D. Day-Lewis was a co-PI on this project).*

Manuscripts in preparation

Kohler, M. and G.P. Curtis, Uranium desorption from contaminated sediments: batch and column studies. To be submitted to the Journal of Contaminant Hydrology,

Kannappan, R. Kohler, M. Miller,A.W. D. R. Rodriguez G.P. Curtis, Uranium desorption from contaminated sediments: intermediate scale studies. To be submitted to the Journal of Contaminant Hydrology

Curtis, G.P., Briggs, M.A. and F.D. Lewis, Prediction of the reactive transport of uranium in tracer tests using batch and geophysical measurements, To be submitted to the Environmental Science and Technology.

6. References

Davis, J. A., and Kent, D. B., 1990, Surface complexation modeling in aqueous geochemistry: in Hochella, M. F., and White, A. F., eds., Mineral-water Interface Geochemistry, Reviews in Mineralogy, v. 23, pp. 177-260.

Greskowiak, J, et al. " Simulating adsorption of U (VI) under transient groundwater flow and hydrochemistry: Physical versus chemical nonequilibrium model (doi 10.1029/2010WR010118)." Water Resources Research 47.8 (2011).

Guillaumont, R. T. Fanghänel, J. Fuger, I. Grenthe, V. Neck, D. A. Palmer and M. H. Rand,2003,Update on the Chemical Thermodynamics of Uranium, Neptunium, Plutonium, Americium and Technetium, Chemical Thermodynamics Series Volume 5, downloaded from https://www.oecd-nea.org/dbtdb/pubs/vol5-update-combo.pdf, September, 2014.

Haggerty, R., and S. M. Gorelick (1995), Multiple-Rate Mass Transfer for Modeling Diffusion and Surface Reactions in Media with Pore-Scale Heterogeneity, Water Resour. Res., 31(10),2383–2400, doi:10.1029/95WR10583.

Harbaugh, A.W., 2005, MODFLOW-2005, the U.S. Geological Survey modular ground-water model -- the Ground-Water Flow Process: U.S. Geological Survey Techniques and Methods 6-A16.

Miller,A.W. D. R. Rodriguez, and B. D. Honeyman, Simplified behaviors from increased heterogeneity: I. 2-D uranium transport experiments at the decimeter scale, Journal of Contaminant Hydrology, Volume 148, May 2013, Pages 39-50.

Poeter, E.P., Hill, M.C., Banta, E.R., Mehl, Steffen, and Christensen, Steen, 2005, UCODE_2005 and Six Other Computer Codes for Universal Sensitivity Analysis, Calibration, and Uncertainty Evaluation: U.S. Geological Survey Techniques and Methods 6-A11, 283p.

USEPA, 2012, Radionuclides in Drinking Water, http://water.epa.gov/lawsregs/rulesregs/sdwa/radionuclides/index.cfm, accessed 23 February, 2015.